Design and analysis of an electro-mechanical impact sensor with an all-ways action mechanism and a Hall sensor

Xuan Son Bui[a], *Van Gion* Do[b], *Duc Hung* Pham[c]

Le Quy Don Technical University, Faculty of Special Equipment, Hanoi, Socialist Republic of Vietnam

[a] e-mail: buixuanson@lqdtu.edu.vn,
ORCID iD: https://orcid.org/0000-0003-4520-5168

[b] e-mail: dovangion@lqdtu.edu.vn, **corresponding author**,
ORCID iD: https://orcid.org/0000-0001-8719-4984

[c] e-mail: hungthoi75@gmail.com,
ORCID iD: https://orcid.org/0009-0008-5645-5596

https://doi.org/10.5937/vojtehg74-59737

FIELD: mechanical engineering
ARTICLE TYPE: original scientific paper

Abstract:

Introduction/purpose: The paper proposes an electro-mechanical impact sensor for grenade detonation using an all-ways action mechanism with permanent magnets and a Hall sensor. After experimental validation, a mathematical model assesses how structural parameters, such as activation threshold, inertial mass, and Hall sensor placement, affect the fuse's sensitivity. The study provides recommendations for optimal sensor design to ensure reliable activation at all impact angles.

Methods: The study used a combined approach to address the problem. Dynamic equations of the all-ways action mechanism were solved using the Runge-Kutta method, the magnetic field was simulated with FEMM 4.2 software, and the Hall voltage variation over time was analyzed to assess the fuse's sensitivity under grenade impact conditions.

Results: The results show that an activation threshold below 80 mV ensures reliable operation at any impact angle with an impact velocity not greater than 2.5 m.s^{-1}. The mass of the inertial object has a significant impact on the sensitivity, more than the mass of the magnet, and the location of the Hall sensor is critical, with some locations providing stable sensitivity and others resulting in poor performance.

Conclusion: The hybrid method presented in this paper effectively studies the signal from an electro-mechanical impact sensor combining an all-ways action mechanism, permanent magnets, and a Hall sensor. The research results are useful contributions to the design of impact sensors in grenade fuses.

Key words: electro-mechanical impact sensor, all-ways action mechanism, Hall effect sensor.

Introduction

Contact with the target is the simplest and affords the most direct solution to the fuzing problem (Headquaters of United States Army Materiel Command, 1969). Nowadays, electro-mechanical sensors have become a common trend, as these alternatives allow for a more compact explosive chain, enhanced control capabilities, and flexible parameter adjustments before use, reducing the size and mass of the fuse. Therefore, they have been applied in many types of ammunition, including grenade fuses.

This paper proposes an electro-mechanical impact sensor for a grenade fuse that consists of an all-ways action mechanism that carries ring permanent magnets and an analog signal Hall sensor, as shown in Figure 1. Each inertial body is equipped with a ring-shaped permanent magnet that moves relative to the fuse body and closer to each other when inertial force acts on the pair of inertial bodies. A Hall sensor is mounted at fixed positions on the fuse body.

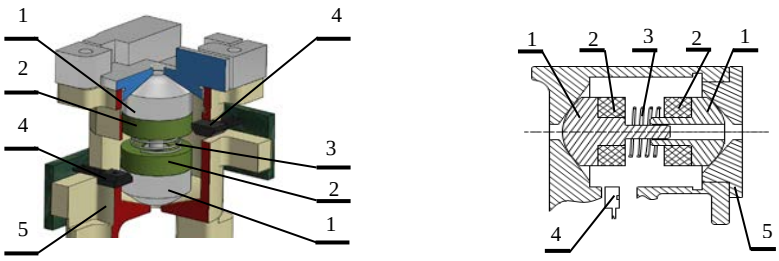

Figure 1 - The structure diagram of the electro-mechanical impact fuse used for hand grenade: *1. The inertial body; 2. Ring permanent magnet; 3. Spring; 4. Hall sensor; 5. fuse body*

With such a structure, when the grenade collides with the media, the inertial bodies move under the action of inertial forces caused by the reaction force of the media and, simultaneously, move the magnets and cause the Hall voltage to change. If the change in the Hall voltage exceeds the activation threshold set in the drive program, the microprocessor will send a signal to detonate the fuse.

To further study the working characteristics of the proposed sensor, the paper incorporates magnetic interaction force into the dynamic model of the all-ways action mechanism. The program for solving the dynamic model for the All-ways action mechanism is linked with the FEMM 4.2 program to simulate the impact sensor signal during grenade operation. The accuracy of the impact sensor signal simulation program is validated through experimental testing. Then, the simulation program is used to

evaluate the influence of some structural parameters on the sensitivity of the proposed impact sensor.

Establishing the program to calculate the output signal of the impact sensor

The Hall voltage calculation program was developed in three steps: (1) establishing the dynamic model of the mechanism, (2) incorporating the magnetic force of the ring magnets, and (3) simulating the magnetic field and calculating the Hall voltage.

The dynamics model of the all-ways action mechanism

The structure and some dimensions of the inertial bodies of the all-ways action mechanism in the proposed electro-mechanical impact sensor are shown in Figure 2.

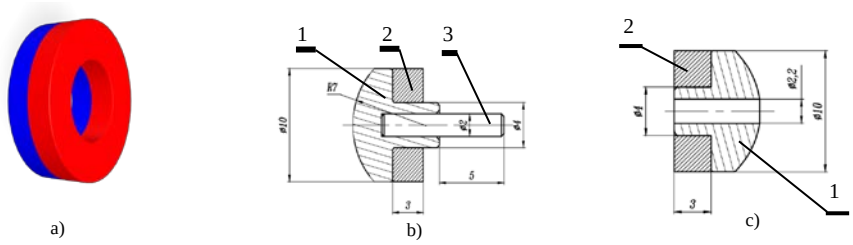

Figure 2 - Type of ring magnet and some dimensions of inertial bodies of the all-ways action mechanism in impact sensor: *a) The magnetic pole of the ring magnet; b) the inertial body 1; c) the inertial body 2*
1. Inertial body; 2. Ring magnet; 3. Guide pillar

The method for establishing the dynamic model of this mechanism is the same as that of the all-ways action mechanism in the URG-86 grenade fuse, as shown in Xuan Son Bui et al. (2021). The forces acting on all the bodies of the mechanism in the general case are shown in Figure 3 and Figure 4.

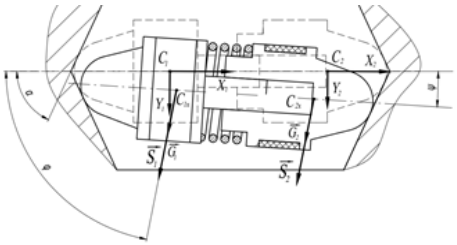

Figure 3 – Some geometric symbols and forces acting on all the bodies of all-ways action mechanism during impact in the general case

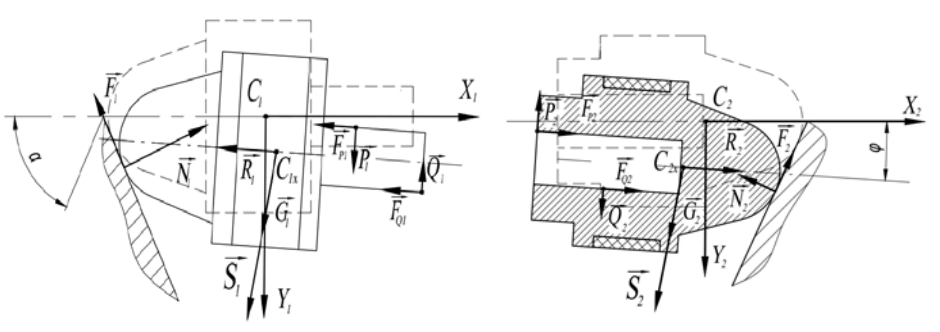

Figure 4 - Forces acting on each body of the all-ways action mechanism during impact in the general case

The dynamic equilibrium equations of all inertial bodies are:

$$\begin{cases} m_1 \dfrac{d\vec{v}_1}{dt} = \vec{S}_1 + \vec{G}_1 + \vec{N}_1 + \vec{F}_1 + \vec{R}_1 + \vec{P}_1 + \vec{Q}_1 + \vec{F}_{P1} + \vec{F}_{Q1} \\ B_1 \dfrac{d^2\psi_1}{dt^2} = \sum\limits_{(i)} M_{1i} \\ m_2 \dfrac{d\vec{v}_2}{dt} = \vec{S}_2 + \vec{G}_2 + \vec{N}_2 + \vec{F}_2 + \vec{R}_2 + \vec{P}_2 + \vec{Q}_2 + \vec{F}_{P2} + \vec{F}_{Q2} \\ B_2 \dfrac{d^2\psi_2}{dt^2} = \sum\limits_{(i)} M_{2i} \end{cases}, \qquad (1)$$

where m_1, m_2 $\dfrac{d\vec{v}_2}{dt}$ and $\dfrac{d\vec{v}_1}{dt}$ are the mass and the acceleration of the inertial bodies 1 and 2, respectively. With $i = (1, 2)$, $\vec{S}_i$ and $\vec{G}_i$ are the inertial forces and gravitational forces; $\vec{N}_i$ are the reaction normal forces of the driving face on the body; $\vec{F}_i$ are friction forces; $\vec{R}_i$ are elastic forces of the springs acting on inertial bodies 1 and 2, respectively; $\vec{P}_i$, $\vec{Q}_i$ and $\vec{F}_{Pi}$, $\vec{F}_{Qi}$ are internal forces between the two bodies; ψ_i are the rotations of the corresponding body 1 or 2; B_i are the moments of inertia about the axis passing through the center of gravity and perpendicular to the motion plane of the inertial bodies 1 and 2. M_{1i} and M_{2i} are moments of the forces acting on each inertial bodies 1 and 2 about the axis passing through the

center of gravity and perpendicular to the motion plane of the inertial body 1 or 2.

These equations have more variables than the number of equations, so we need to add some constraint equations before solving. The constraint equations are:

$$\Delta_x = C_1C_2 - C_{1x}C_{2x} = C_1C_2 - \frac{C_1C_2 - x_1 + x_2}{\cos\psi}, \quad (2)$$

$$\psi_1 = \psi_2 = \psi, \quad (3)$$

$$\tan\psi = \frac{y_2 - y_1}{C_1C_2 - x_1 + x_2}, \quad (4)$$

$$y_1 = \left(x_1 + O_1C_1 - O_1C_1\cos\psi\right)\tan\alpha + O_1C_1\sin\psi, \quad (5)$$

$$y_2 = \left(O_1C_1 - O_1C_1\cos\psi - x_2\right)\tan\alpha - O_1C_1\sin\psi, \quad (6)$$

where, x_1, x_2, y_1 and y_2 are the displacements of the center of gravity of the inertial bodies 1 and 2 along the axes of the coordinate system. C_1C_2 and $C_{1x}C_{2x}$ are the distances between the gravity centers of the two bodies at the initial time and the considered time of the impact process, whereas O_1C_1 and O_2C_2 are the distances between the center of gravity and the center of the hemisphere in the two bodies, respectively. Some characteristic points and geometric parameters of the all-ways action mechanism in the proposed sensor used in constraint equations are shown in Figure 5.

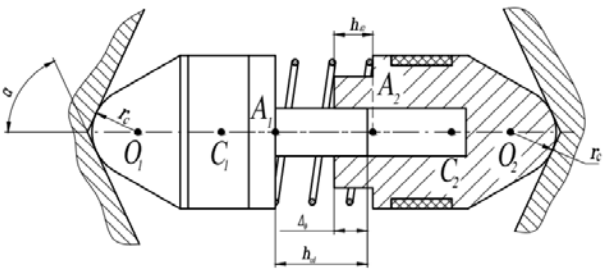

Figure 5 – Some Characteristic points and geometric parameters used in constraint equations

After eliminating all internal forces, we obtain the equations:

$$\begin{cases} \ddot{x}_1 = K_{six1}.\ddot{\psi} - K_{y1x1}.\ddot{y}_1 - K_{y2x1}.\ddot{y}_2 + K_{s2x1}.(S_2 + G_2) + K_{s1x1}.(S_1 + G_1) + K_{rx1}.R \\ \ddot{y}_1 = \tan\alpha.\ddot{x}_1 + O_1C_1.\tan\alpha.\left(\sin\psi.\ddot{\psi} + \cos\psi.\dot{\psi}^2\right) + O_1C_1.\left(\cos\psi.\ddot{\psi} - \sin\psi.\dot{\psi}^2\right) \\ \ddot{x}_2 = K_{six2}\ddot{\psi} + K_{y1x2}\ddot{y}_1 + K_{y2x2}\ddot{y}_2 - K_{s2x2}(S_2 + G_2) - K_{s1x2}(S_1 + G_1) + K_{rx2}R \\ \ddot{y}_2 = -\tan\alpha.\ddot{x}_2 + O_2C_2.\tan\alpha.\left(\sin\psi.\ddot{\psi} + \cos\psi.\dot{\psi}^2\right) - O_2C_2.\left(\cos\psi.\ddot{\psi} - \sin\psi.\dot{\psi}^2\right), \\ \ddot{\psi} = \cos^2\psi.\left\{\dfrac{\ddot{y}_2 - \ddot{y}_1}{C_1C_2 - x_1 + x_2} + \dfrac{\left(\ddot{x}_1 - \ddot{x}_2\right)\left(y_2 - y_1\right) + 2\left(\dot{x}_1 - \dot{x}_2\right)\left(\dot{y}_2 - \dot{y}_1\right)}{\left(C_1C_2 - x_1 + x_2\right)^2}\right\} \\ + \dfrac{2.\left(\dot{x}_1 - \dot{x}_2\right).\left(\dot{x}_1 - \dot{x}_2\right).\left(y_2 - y_1\right)}{\left(C_1C_2 - x_1 + x_2\right)^4}.\cos^2\psi - \dfrac{2\sin\psi.\dot{\psi}^2}{\cos\psi} \end{cases} \quad (7)$$

where, K_{xy} (x=[x_1, y_1, x_2, y_2, ψ, S_1, S_2, R], y=[x_1, y_1, x_2, y_2, ψ], $x \neq y$) are reduction coefficients.

Using the same method for these cases, as shown in Figure 6, we apply the dynamic model for the all-ways action mechanism in all impact angles.

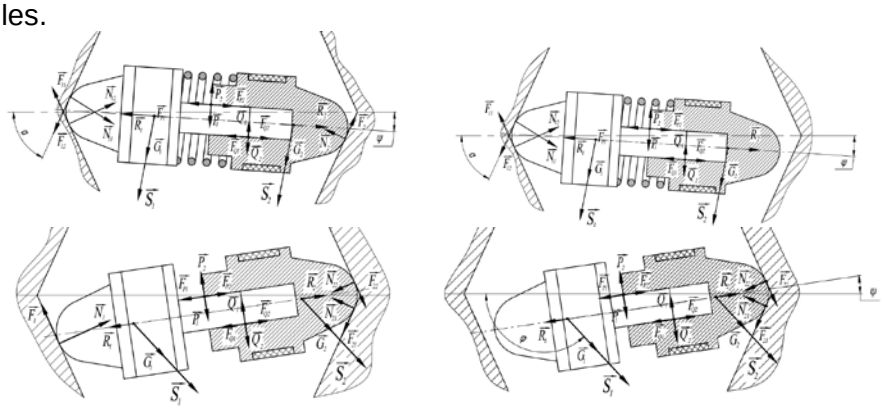

Figure 6 - All other working cases of the all-ways action mechanism

The elastic force $\vec{R}$ can be calculated using the following formula:

$$R = k.(\lambda_0 + \Delta_x), \quad (8)$$

where, R is the spring elastic force, k is the stiffness of the spring, λ0 is the initial compression of the spring, and Δ_x is the relative displacement between the two inertial bodies, calculated by equation (2).

The inertial force acting on each inertial body is:

$$S_i = m_i.\frac{dV(t)}{dt}, \quad (9)$$

where *V(t)* is the velocity function of the grenade over time upon impact.

The paper concentrates on analyzing the operation of the impact sensor in a grenade during impact with the concrete ground. The authors conducted a drop test examining the impact of a grenade on concrete, utilizing the method presented in Martin Macko et al. (2024). The tests were performed with initial velocities below 5 m.s^{-1}, and the velocity of the grenade during impact was recorded using a high-speed camera. Several time-based regression functions were used to approximate the grenade's velocity from the test results. After evaluating the various options, the most accurate approximation of the grenade's velocity upon impact was found to be represented by a specific expression:

$$V(t) = \frac{1}{2}(1-\beta_{con})V_i + \frac{1}{2}(1+\beta_{con})V_i \cos(\Omega_{con}t), \tag{10}$$

The coefficients for this expression were determined based on the initial impact velocity using polynomial functions:

$$\beta_{con} = 0,0053V_i^2 - 0,1113V_i - 2,3094\,, \tag{11}$$

$$\Omega_{con} = 14,082V_i^2 - 356,56V_i + 4446,1\,, \tag{12}$$

If the initial grenade impact velocity is higher than 5 m.s^{-1}, the velocity function proposed by D.M.Komarov is used as used in Xuan Son Bui et al. (2021) and K. Phanthavong et al. (2023). In the case of impact with concrete media, the coefficient $\beta = 0.45$ and the frequency Ω are calculated using the following formula:

$$\Omega = \frac{\pi}{t_V}\,, \tag{13}$$

where t_V is the total impact time calculated from the ratio $\frac{V_V}{t_V} = 6.10^3$.

Adding the magnetic force of the pair of ring magnets in the dynamic model of the all-ways action mechanism

In the proposed impact sensor, the two magnets are positioned so that their like poles point toward each other, and the magnetic force between them is repulsive. This repulsive force is calculated using the surface electric method, as demonstrated in K. Yuan et al. (2019). Figure 7 illustrates the model of the pair of magnets.

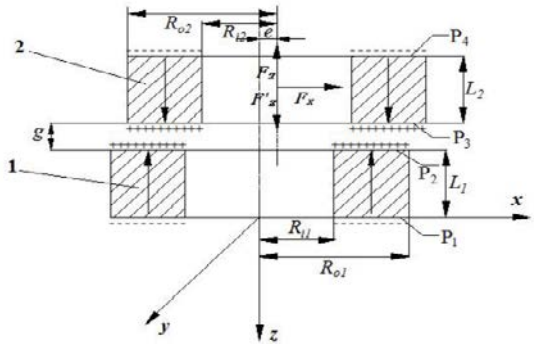

Figure 7 - Model of the interaction force between the pair of ring magnets

The magnetic forces between the faces are calculated using the following equations (K. Yuan et al, 2019):

$$F_{14,z} = \frac{B_r^2}{4\pi\mu_0} \int_0^{2\pi}\int_0^{2\pi}\int_{R_{i1}}^{R_{o1}}\int_{R_{i2}}^{R_{o2}} \frac{(L_1 + g + L_2).r_1.r_4 dr_1 dr_4 d\alpha d\beta}{\left[(L_1 + g + L_2)^2 + (r_1\cos\alpha - r_4\cos\beta - e)^2 + (r_1\sin\alpha - r_4\sin\beta)^2\right]^{3/2}} \quad (14)$$

$$F_{13,z} = \frac{B_r^2}{4\pi\mu_0} \int_0^{2\pi}\int_0^{2\pi}\int_{R_{i1}}^{R_{o1}}\int_{R_{i2}}^{R_{o2}} \frac{(L_1 + g).r_1.r_3 dr_1 dr_3 d\alpha d\beta}{\left[(L_1 + g)^2 + (r_1\cos\alpha - r_3\cos\beta - e)^2 + (r_1\sin\alpha - r_3\sin\beta)^2\right]^{3/2}} \quad (15)$$

$$F_{23,z} = \frac{B_r^2}{4\pi\mu_0} \int_0^{2\pi}\int_0^{2\pi}\int_{R_{i1}}^{R_{o1}}\int_{R_{i2}}^{R_{o2}} \frac{(g).r_2.r_3 dr_2 dr_3 d\alpha d\beta}{\left[(g)^2 + (r_2\cos\alpha - r_3\cos\beta - e)^2 + (r_2\sin\alpha - r_3\sin\beta)^2\right]^{3/2}} \quad (16)$$

$$F_{24,z} = \frac{B_r^2}{4\pi\mu_0} \int_0^{2\pi}\int_0^{2\pi}\int_{R_{i1}}^{R_{o1}}\int_{R_{i2}}^{R_{o2}} \frac{(L_2 + g).r_2.r_4 dr_2 dr_4 d\alpha d\beta}{\left[(L_2 + g)^2 + (r_2\cos\alpha - r_4\cos\beta - e)^2 + (r_2\sin\alpha - r_4\sin\beta)^2\right]^{3/2}} \quad (17)$$

The summary repulsive force acting on each magnet can be calculated by the equation:

$$F_z = F_{14,z} - F_{13,z} + F_{23,z} - F_{24,z} \quad (18)$$

The impact sensor uses magnets made from N35-NdFeB. The magnetic parameters of this magnetic material are shown in Table 1 (Arnold magnetic technologies, 2021).

Table 1 - Magnetic parameters of NdFeB magnetic material N35

Parameter	Symbol	Unit	Value
Residual induction	B_r	T	1.12
Coercivity	H_{cb}	kA/m	836
Intrinsic coercivity	H_c	kA/m	955
Maximum energy product	$(BH)_{max}$	K.J/m^3	239

The change in the magnetic interaction force of the pair of ring magnets is shown in Figure 8.

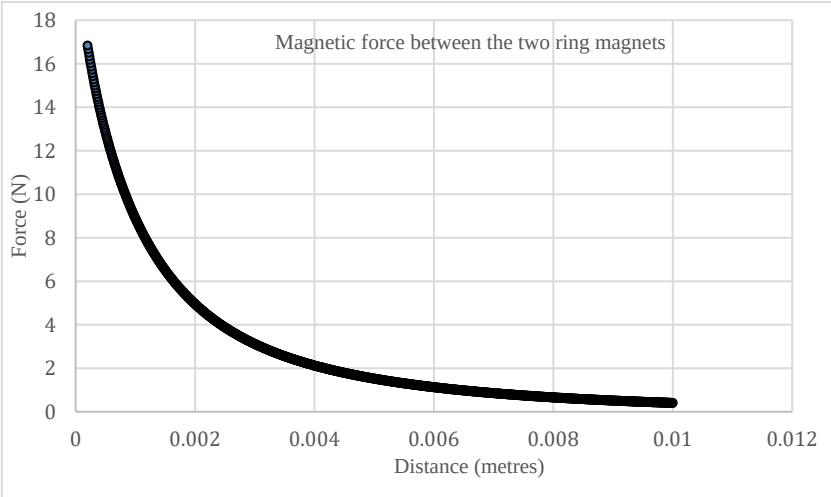

Figure 8 - The magnetic interaction force of the pair of ring magnets in the impact sensor depending on the distance

When adding the magnetic interaction force between the two magnets, we obtain the equations in the general case as shown:

$$\begin{cases} \ddot{x}_1 = K_{six1}\ddot{\psi} - K_{y1x1}\ddot{y}_1 - K_{y2x1}\ddot{y}_2 + K_{s2x1}(S_2+G_2) + K_{s1x1}(S_1+G_1) + K_{rx1}(R+\boldsymbol{F_{mg}}) \\ \ddot{y}_1 = \tan\alpha.\ddot{x}_1 + O_1C_1\tan\alpha\left(\sin\psi.\ddot{\psi} + \cos\psi.\dot{\psi}^2\right) + O_1C_1.\left(\cos\psi.\ddot{\psi} - \sin\psi.\dot{\psi}^2\right) \\ \ddot{x}_2 = K_{six2}\ddot{\psi} + K_{y1x2}\ddot{y}_1 + K_{y2x2}\ddot{y}_2 - K_{s2x2}(S_2+G_2) - K_{s1x2}(S_1+G_1) + K_{rx2}(R+\boldsymbol{F_{mg}}) \\ \ddot{y}_2 = -\tan\alpha.\ddot{x}_2 + O_2C_2\tan\alpha\left(\sin\psi.\ddot{\psi} + \cos\psi.\dot{\psi}^2\right) - O_2C_2.\left(\cos\psi.\ddot{\psi} - \sin\psi.\dot{\psi}^2\right) \\ \ddot{\psi} = \cos^2\psi.\left\{\dfrac{\ddot{y}_2-\ddot{y}_1}{C_1C_2-x_1+x_2} + \dfrac{(\ddot{x}_1-\ddot{x}_2)(y_2-y_1)+2(\dot{x}_1-\dot{x}_2)(\dot{y}_2-\dot{y}_1)}{(C_1C_2-x_1+x_2)^2}\right\} \\ +\dfrac{2.(\dot{x}_1-\dot{x}_2)(\dot{x}_1-\dot{x}_2)(y_2-y_1)}{(C_1C_2-x_1+x_2)^4}.\cos^2\psi - \dfrac{2\sin\psi.\dot{\psi}^2}{\cos\psi} \end{cases} \quad (19)$$

where $\boldsymbol{F_{mag}}$ is the magnetic interaction force calculated using equation (18).

Doing the same for all other cases, the dynamic model of the all-ways action mechanism in the electro-mechanical impact sensor is established. This dynamic model can be solved using the ODE45 function in MATLAB software, and the output results are the kinematic parameters of the two inertial bodies, such as displacements, velocities, and accelerations, depending on the impact angle and collision velocity conditions.

Calculating the impact sensor output signal using the dynamic model of the all-ways action mechanism and the FEMM 4.2 program

The program to solve the all-ways action mechanism's dynamic model is combined with FEMM 4.2 software to build a model of the pair of magnets and determine the magnetic flux density. From that, the output signal of the impact sensor can be calculated. The model and simulation results for the impact sensor at one specific time step are illustrated in Figure 9.

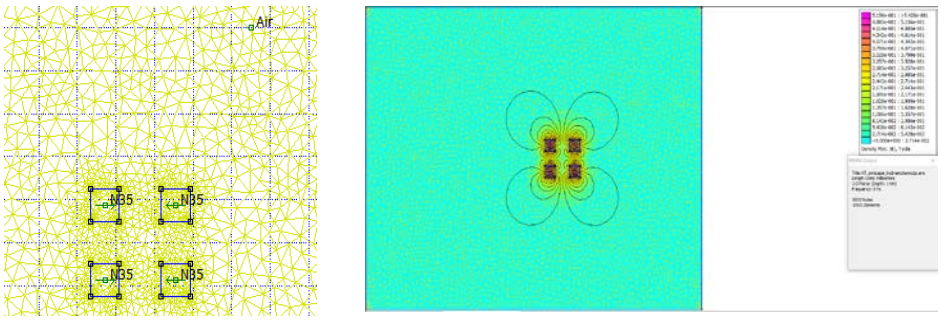

Figure 9 - The model and the magnetic field of the pair of magnets in FEMM 4.2

Figure 10 displays the variation in magnetic flux density and the output of the Hall voltage from the sensor during a grenade impact scenario.

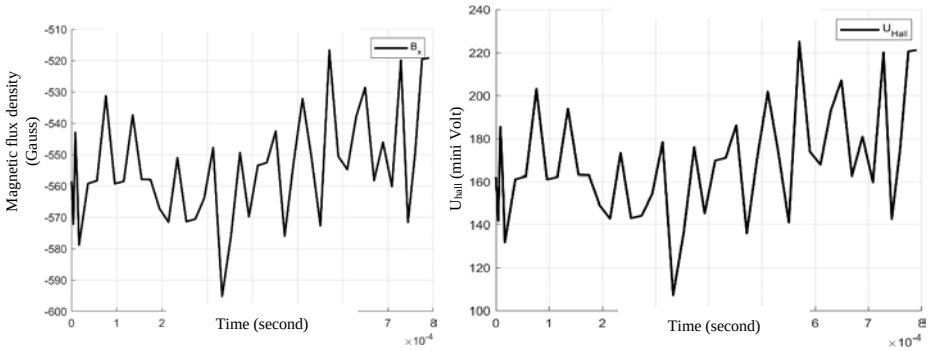

Figure 10 - Change of magnetic flux density and the Hall voltage of proposed sensor

Testing to evaluate the accuracy of the results obtained from the established program

An experiment was carried out to assess the accuracy of the developed mathematical model for the impact sensor to measure the sensor's output signal, as shown in Figure 11.

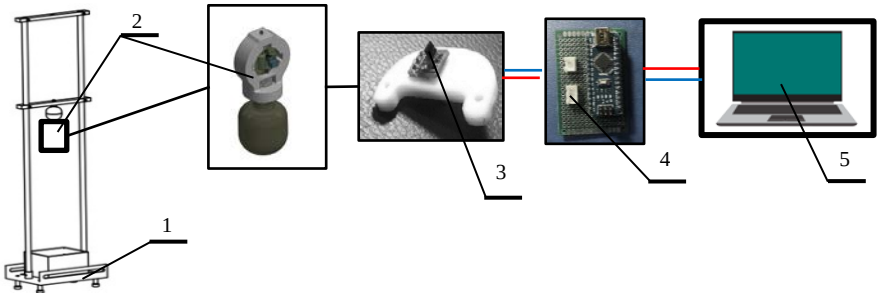

Figure 11 - Assembly of equipment to measure the Hall voltage of the impact sensor during the grenade impact on concrete: *1. The frame; 2. The grenade body with the impact sensor; 3. Circuit with the Hall sensor; 4. The measuring and signal conversion circuit; 5. The computer*

Some dimensions of the inertial bodies are illustrated in Figure 2, and three samples of the proposed impact sensor were fabricated. The mass of the inertial bodies for each sample is presented in Table 2.

Table 2 - Mass of three different samples for the test of math model accuracy

	Mass of the inertial body 1 (gram)	Mass of the inertial body 2 (gram)
Sample 1	1.92	1.57
Sample 2	1.95	1.58
Sample 3	1.87	1.56

The grenade body was released from a height of 0.87 m, resulting in an initial impact velocity of 4.1 $m.s^{-1}$ upon striking a concrete block. A test impact sensor was positioned on an angle-adjustable mechanism to align with the impact angle of the all-ways action mechanism during the test. Figure 12 illustrates the setup and the measured data from one test angle.

Figure 12 - Set up and measured data of one test case

The Hall sensor used in this impact sensor has code AH49E, and the change of Hall voltage conforms to the change of magnetic flux density when the input voltage is 5 volt, as shown in Figure 13 (Honeywell Inc., 1998; BCD Semiconductor Manufacturing Limited, 2010).

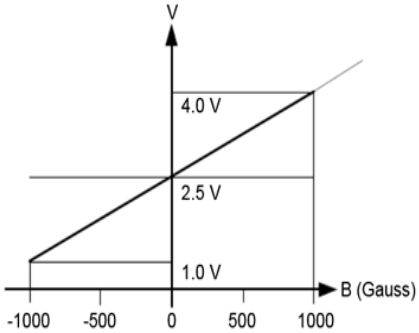

Figure 13 - The change of th Hall voltage as the change of magnetic flux density when input voltage is 5 volts

Figure 14 shows the change of the Hall voltage as a function of the impact time in one experiment.

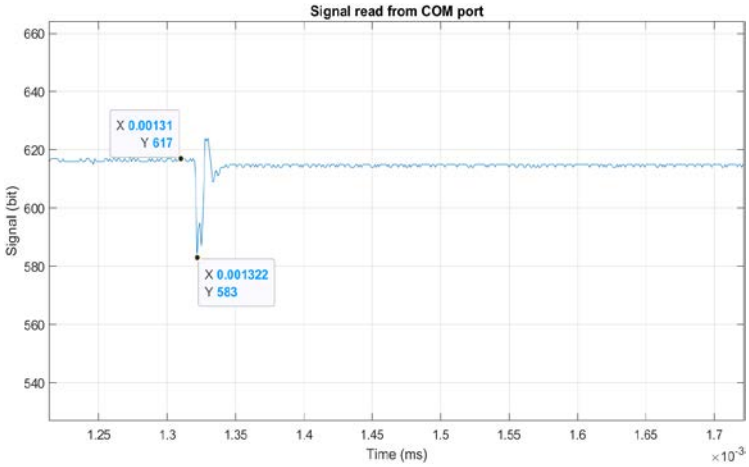

Figure 14 - The change of impact sensor signal over time in one measurement case

The experimental results and the calculation results obtained from the developed program simulate the output signal of the impact sensor in the given setup, as shown in Figure 15.

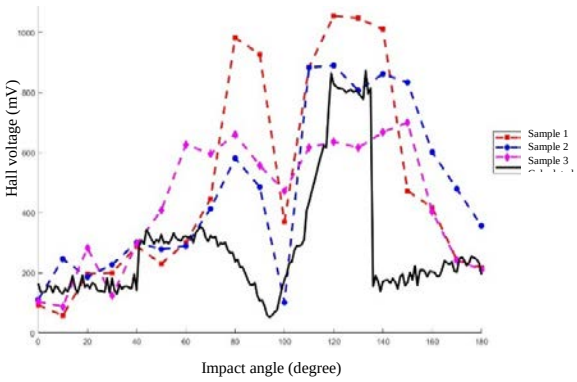

Figure 15 - Comparing the Hall voltage measured in the experiment and the theoretical calculation results for the impact sensor

The results show that the program for determining the signal of the electro-mechanical impact sensor in the grenade fuse is relatively accurate. The program can be used to study the operation of the proposed impact sensor in the grenade fuse.

Evaluation of the influence of the magnetic force of the pair of ring magnets on the dynamic characteristics of the all-ways action mechanism

Figure 16 and Figure 17 compare the maximum relative displacement between the inertial bodies and the maximum rotation angle of the mechanism at various impact angles in the range from 0° to 180° and velocities, both with and without the magnetic force.

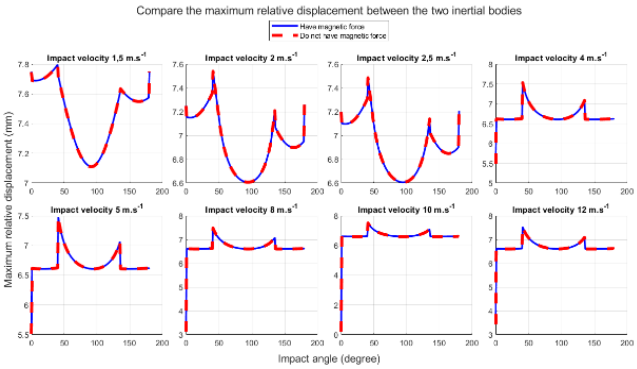

Figure 16 – Comparison of the maximum relative displacement of the two inertial bodies with and without the magnetic force at some cases of impact velocities

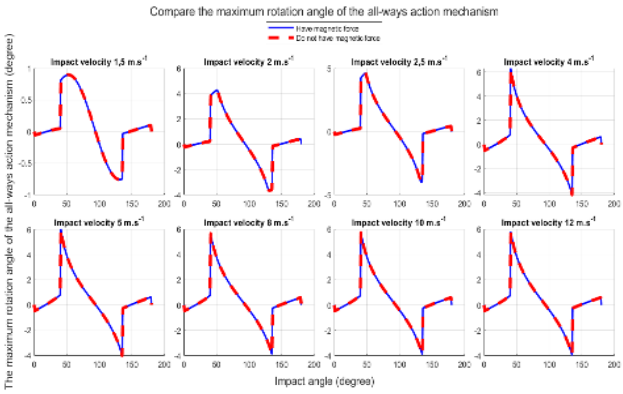

Figure 17 - Comparison of the maximum rotation angle of the all-ways action mechanism with and without the magnetic force at some cases of impact velocities

The comparison results show that the magnetic interaction force between the two magnets mounted on the two inertial bodies has very little effect on the kinematics of the inertial blocks. This is becaise the value of this interaction force is relatively small, being smaller than the elastic force of the compression spring in the all-ways action mechanism of the impact grenade fuse. Meanwhile, the effect of the elastic force of the compression spring on the kinematics of the inertial bodies is not very large (Xuan Son Bui et al, 2021), so the effect of the magnetic interaction force on the kinematics of the inertial bodies is also negligible.

The change of the impact sensor signal when the all-ways action mechanism works with the impact process of the grenade

The Hall sensor works with a magnetic field perpendicular to the surface of the Hall plate, corresponding to the OX direction of the coordinate system in the dynamic model setup of the all-ways action impact mechanism. To evaluate the influence of the kinematics of inertial masses on the change of electro-mechanical sensor signals, this paper compares the change in the maximum value of the Hall voltage deviation generated by the sensor at different contact angles with the change in the initial velocity of the grenade when it impacts the concrete media. The calculation results are shown in Figure 18.

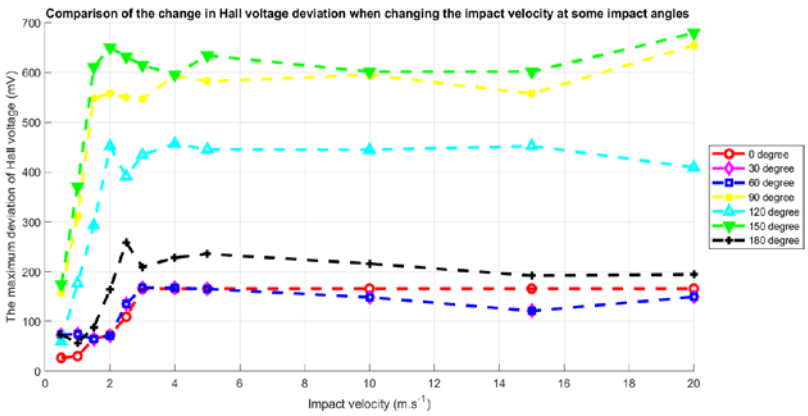

Figure 18 - Comparison of the change of the Hall voltage at an impact angle while changing the impact velocity

The calculated results show that the change level in the Hall voltage deviation at different impact angles is different and depends greatly on the impact velocity. However, it can be seen that in the impact velocity region below 4 $m.s^{-1}$, the Hall voltage deviation increases sharply when the impact velocity of the grenade with the ground increases. However, when the impact velocity is greater than 4 $m.s^{-1}$, the Hall voltage deviation changes little with increasing impact velocity.

Investigation of the influence of some structural parameters on the sensitivity of the electro-mechanical impact sensor

In this part, the paper uses the program developed above to calculate the electro-mechanical impact sensor signal and evaluate the effect of the following parameters: the setting threshold of the control program, the mass of the inertial bodies, and the position of the Hall sensor on the sensitivity of the impact sensor.

Setting the threshold of the control program

To determine a suitable threshold for the control program and ensure the required sensitivity of the grenade fuse, this paper investigates how the threshold value affects sensor sensitivity. All sensor parameters are kept constant except for the threshold. Sensitivity is compared based on the minimum impact velocity, at each angle from 0° to 180°, that produces a Hall voltage equal to or greater than the set threshold. The sensor is considered suitably sensitive if the required impact velocity at all angles remains below 2.5 $m.s^{-1}$. Figure 19 and Figure 20 show the sensitivity

diagrams of the electro-mechanical impact sensor with thresholds ranging from 70 mV to 150 mV.

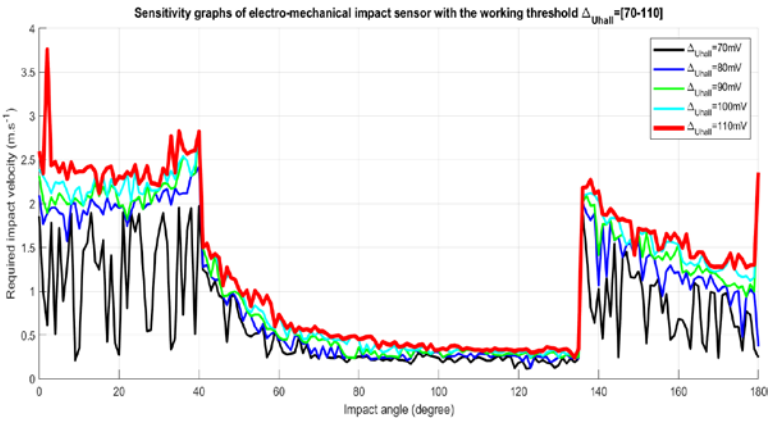

Figure 19 - Sensitivity graphs for cases where the threshold changes from 70 mV to 110 mV

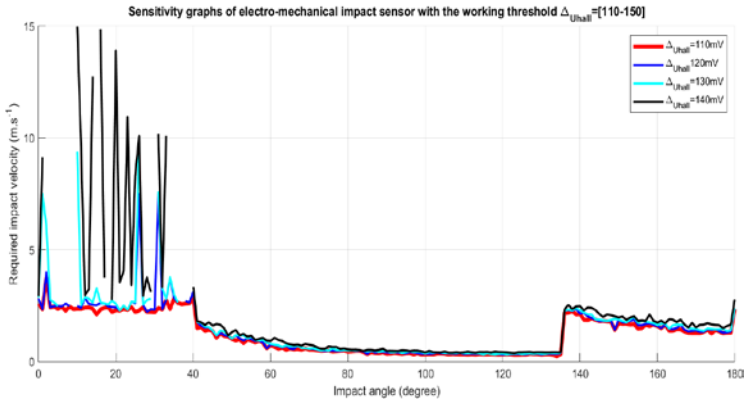

Figure 20 - Sensitivity graphs for cases where the threshold changes from 110 mV to 150 mV

The sensitivity graphs show that with activation thresholds between 70 mV and 110 mV, the sensor can operate at any impact angle with velocities below 4 m.s^{-1}. At thresholds of 120 mV to 150 mV, some angles still show high sensitivity at velocities under 1 m.s^{-1}, but sensitivity is very low for impact angles below 45^{0}. At 130 mV or higher, some angles require impact velocities above 15 m.s^{-1}. Figure 21 compares the ratio of impact angles at which the sensor can operate over a range of initial impact velocities of the grenade.

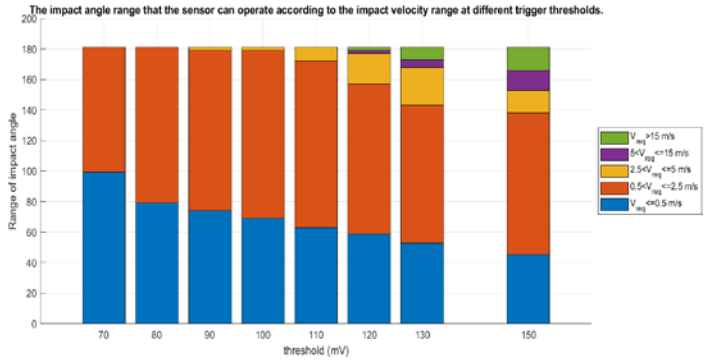

Figure 21 – Comparison of the range of impact angles at which the impact sensor can operate for different impact velocity ranges and activation thresholds

The chart shows that when the activation threshold is below 80 mV, the sensor works at 100% of impact angles with velocities under 2.5 m.s^{-1}. At a 70 mV threshold, 55.8% of impact angles work below 0.5 m.s^{-1}, while at 80 mV, it drops to 43.6%. For activation thresholds of 90 mV and 100 mV, the figures are 40.9% and 38.1%, respectively, with a small proportion (about 1.1%) requiring velocities between 2.5 m.s^{-1} and 5 m.s^{-1}. At 110 mV, this increases to 5%, and at 120 mV or higher, some angles require velocities over 15 m.s^{-1}.

In conclusion, activation thresholds below 80 mV are recommended to ensure that the sensor meets the sensitivity requirements of an impact grenade. Thresholds of 90 mV and 100 mV still offer acceptable sensitivity, with only a few angles requiring impact velocities higher than 2.5 m.s^{-1}. This study selects 90 mV as the sensor's activation threshold, as it closely matches the required sensitivity across most impact angles.

Mass of the inertial bodies

To study the effect of the mass of these components on the sensor sensitivity, the paper analyzes changes in sensor sensitivity when using different materials. The materials used are listed in Table 3 and Table 4.

Table 3 - Test of the case changes the magnet's material of the two inertial bodies

Test number	1	2	3	4	5
The density of the magnetic material (g.cm^{-3})	4,8	5,0	6,5	6,9	7,55
The density of the inertial body's material (g.cm^{-3})	1,03	1,03	1,03	1,03	1,03
Mass of the first inertial body (gram)	1,46	1,5	1,79	1,87	2,0
Mass of the second inertial body (gram)	1,38	1,42	1,71	1,79	1,92

Table 4 - Test of the case changes the main body's material of the two inertial bodies.

Test number	1	2	3	4	5	6
The density of the magnetic material ($g.cm^{-3}$)	7,55	7,55	7,55	7,55	7,55	7,55
The density of the inertial body's material ($g.cm^{-3}$)	1,03	1,637	2,7	4,73	8,0	8,73
Mass of the first inertial body (gram)	2,002	2,143	2,391	2,812	3,623	3,794
Mass of the second inertial body (gram)	1,922	2,174	2,616	3,37	4,82	5,12

Sensitivity diagrams of the impact sensor for changes in the density of the magnet materialare shown in Figure 22.

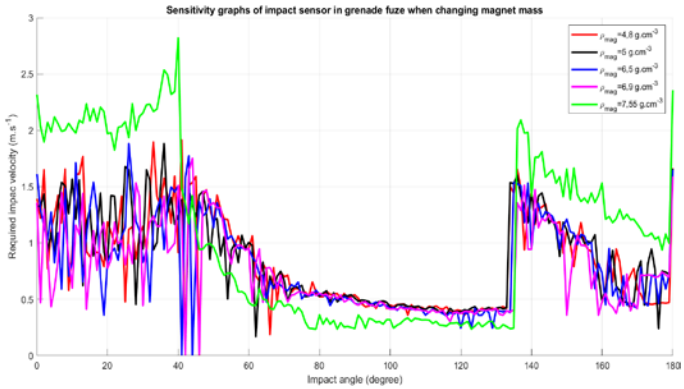

Figure 22 - The sensitivity graphs of the electro-mechanical impact sensor in grenade fuse when changing the mass of magnets.

From the diagram, we can see that when the ring magnet uses a material with a density of less than 6.9 $g.cm^{-3}$, the effect of changes in the magnet mass on the sensitivity of the electro-mechanical impact sensor is insignificant. The sensor can work with a required impact velocity of less than 2 $m.s^{-1}$ in all tested cases. However, when the sensor uses a magnet with a density of up to 7.55 $g.cm^{-3}$, its sensitivity changes significantly and is not uniform. When the density of the magnet block is 7.55 $g.cm^{-3}$, in the impact angle areas below 40^0 and above 136^0, the sensitivity of the impact sensor decreases, the required impact velocity of this range of impact angle increases, and some impact angles require an impact velocity of nearly 3 $m.s^{-1}$. In the impact angle area greater than 41^0 and below 135^0, the sensitivity of the electro-mechanical impact sensor increases when the required impact velocity is smaller than that of the sensor using a magnet with a density of less than 6.9 $g.cm^{-3}$.

By comparing the operating angle range at various impact velocities from 0 to 15 $m.s^{-1}$, we obtain the graph shown in Figure 23.

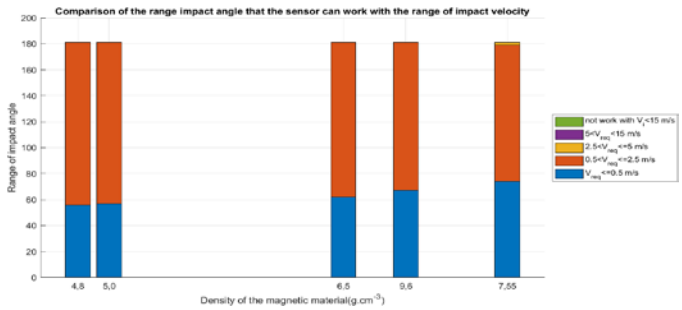

Figure 23 - Comparison of the range of impact angles at which the sensor can operate with the range of impact velocities

While the magnet material has a density of less than 6.9 g.cm^{-3}, approximately 30% of the impact angles allow the impact sensor to operate with an impact velocity of less than 0.5 m.s^{-1}. However, when the density of the magnet changes to 7.55 g.cm^{-3}, the required impact velocity of less than 0.5 m.s^{-1} increases and reaches 40.9%, 58% of the impact angles work with an impact velocity of less than 2.5 m.s^{-1}, but at the same time, some impact angles accounting for about 1% of the total impact angles require an impact velocity of more than 2.5 m.s^{-1} to work reliably.

The change in sensor sensitivity when changing the density of the magnet material is explained by the change in the inertial properties of the inertial masses. When the density of the magnet ring is below 6.9 g.cm^{-3}, the mass of the magnet still accounts for a small proportion of the inertial mass, so the kinematic properties of the sensor are less affected. However, when the density of the magnet ring material is 7.55 g.cm^{-3}, the mass of the magnet accounts for a large proportion of the inertial mass. It changes the kinematic properties of the sensor when colliding, thus significantly reducing its sensitivity.

When changing the main body's material, the impact sensor's sensitivity graphs are shown in Figure 24.

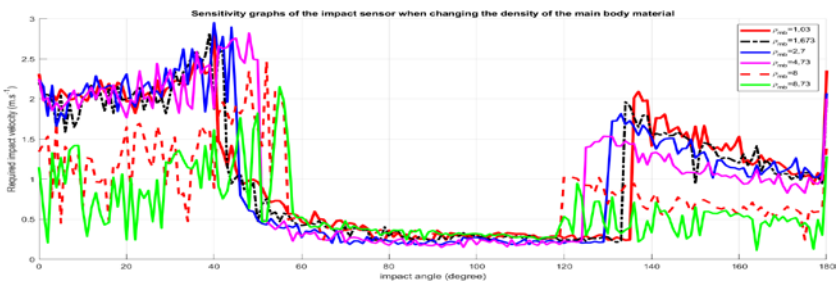

Figure 24 - The sensitivity graphs of the impact sensor when changing the density of the main body of the inertial masses

The sensitivity graphs show that the mass of the main body has a greater impact on sensor sensitivity than the magnet's mass. Increasing the main body's density from 1.03 g.cm^{-3} to 4.73 g.cm^{-3} slightly improves sensitivity, requiring about 3 m.s^{-1} impact velocity for activation at all angles. At 8 g.cm^{-3}, sensitivity significantly improves, lowering the required velocity to 2.5 m.s^{-1}, and at 8.73 g.cm^{-3}, to 2.2 m.s^{-1}.

Density changes also shift sensitivity ranges. At 1.03 g.cm^{-3}, the sensor is less sensitive below 40°, with minimum activation velocity above 1.8 m.s^{-1}. It performs best between 40° and 136°, needing less than 0.25 m.s^{-1} at some angles. Above 137°, sensitivity drops, requiring at least 1 m.s^{-1}. As density increases to 2.7, 4.73, and 8.73 g.cm^{-3}, the high-sensitivity angle range narrows from 43°–134° to 58°–120°.

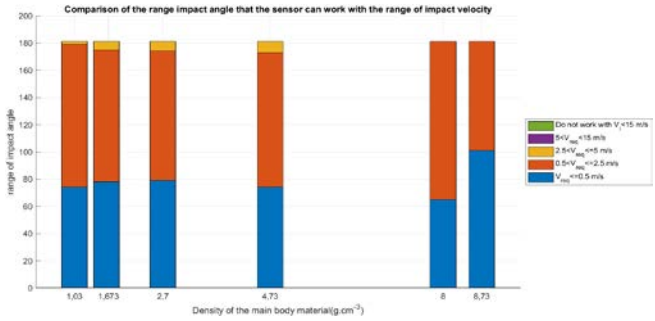

Figure 25 - Comparison of the range of impact angles at which the sensor can operate with the range of impact velocities when changing the material density of the main body

Position of the Hall sensor

To evaluate the influence of the Hall sensor placement on the sensitivity of the electro-mechanical impact sensor, the input parameters for the program were kept constant, including the geometric parameters of the all-ways action mechanism, the activation threshold was 90 mV, the magnet type was NdFeB N35, and the inertial main body's material was plastic with a density of 1.03 g.cm^{-3}. The Hall sensor placement was varied according to several options, as shown in the diagram in Figure 26.

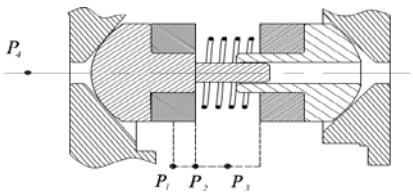

Figure 26 - Diagram of the locations in the study of the influence of Hall sensor placement on the sensitivity of electro-mechanical impact sensor

All study positions are located on the moving plane of the all-ways action mechanism. Position P_1 is on the magnet ring's cross-sectional symmetry axis, P_2 is on the lower edge of the magnet ring near the guide pin, P_3 is on the symmetry axis of two magnets, and P_4 is on the center axis of a magnet pair. At each position, the Hall sensor is placed at specific distances from a reference point. For P_1 to P_3, the reference point is where the study axis intersects the mechanism's symmetry axis. For P_4, it is where the symmetry axis meets the boundary of the magnet head near the guide pin. Distances are listed in Table 5.

Table 5 - Distance from the points where the Hall sensor is placed to the reference point at each sampling position

Point number / Study position	**1**	**2**	**3**	**4**	**5**
P_1	8,5	9,0	9,5	10	12
P_2	8,5	9,0	9,5	10	12
P_3	8,5	9,0	9,5	10	12
P_4	8,0	8,5	9,5	10	12

The sensitivity diagram of the electro-mechanical impact sensor when placing the Hall sensor at the study position P_1 is shown in Figure 27.

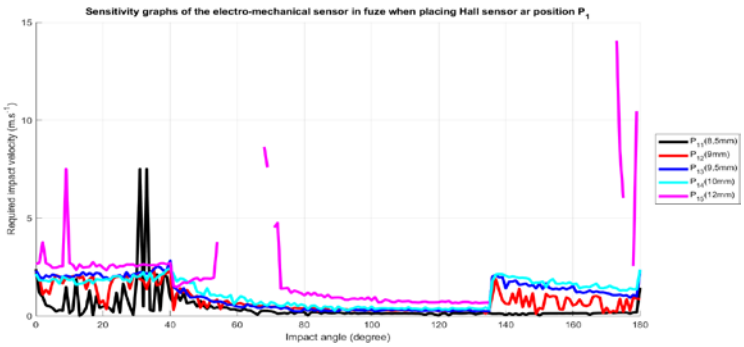

Figure 27- Sensitivity graphs of the impact sensor when placing the Hall sensor at position P_1

The analysis shows that when the Hall sensor is placed at position P_1, the impact sensor has low sensitivity at angles below 60°, where the first inertial body is mostly stationary or rotating, and the second moves toward it. Between 60° and 135°, where both inertial bodies move, the sensor is most sensitive and requires the lowest impact velocities. Above 135°, sensitivity decreases but remains better than below 60°.

At position P_{11}, the sensor shows very high sensitivity, needing less than 1 m.s^{-1} impact velocity at almost all angles, except between 31° and 33°, where over 7 m.s^{-1} is required. At P_{12} and P_{13}, sensitivity is more balanced—slightly lower where both bodies move, but higher in other ranges. At P_{14}, sensor sensitivity drops significantly, with some angles requiring more than 15 m.s^{-1} for activation.

When comparing the required impact velocities in the maximum, minimum, and average values for the working impact angle ranges with impact velocities below 15 m.s^{-1}, we obtain the graph shown in Figure 28.

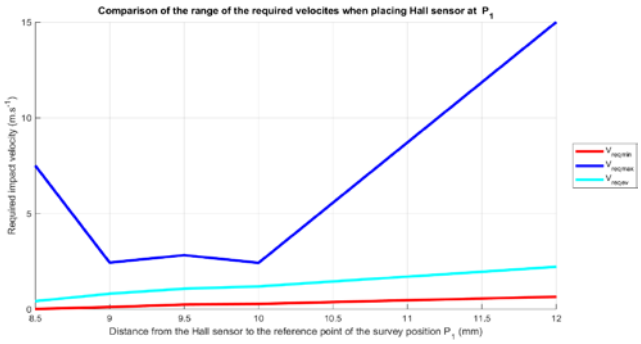

Figure 28 - Comparison of the range of required impact velocities when placing the Hall sensor at position P_1

When the Hall sensor is set at P_{11}, the minimum required impact velocity is very low, but the maximum required impact velocity is as high as 7.5 m.s^{-1}. When the Hall sensor is set at any P_{12}, P_{13}, or P_{14}, all require contact velocities less than 3.5 m.s^{-1}. If the Hall sensor is set at P_{15}, many impact angles require impact velocities close to 15 m.s^{-1} to function.

The sensitivity graphs and the graph to compare the impact angles of the impact velocity range of the impact sensor when placing the Hall sensor at the sampling points of position P_2 are shown in Figure 29.

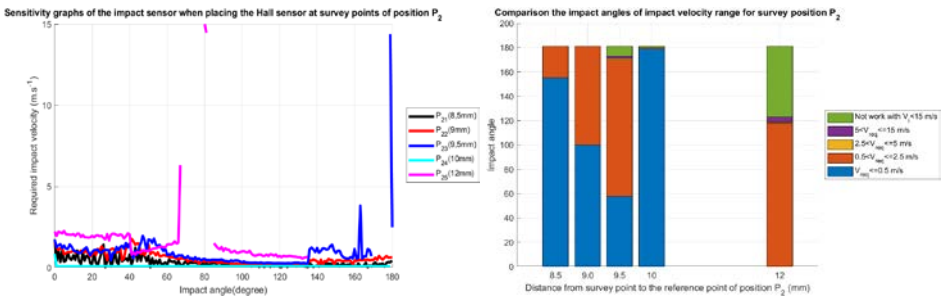

Figure 29 - The sensitivity graphs and comparison of the range of impact angles with different impact velocities when placing the Hall sensor at the position P_2

The sensor sensitivity diagram shows that when the Hall sensor is placed at P_{21} and P_{22}, the impact sensor has a very high sensitivity as it only needs an impact velocity of 1.79 $m.s^{-1}$ to operate at any impact angle. When the Hall sensor is placed at P_{23}, the sensitivity of the impact sensor decreases as the electro-mechanical impact sensor cannot operate at an impact velocity below 15 $m.s^{-1}$ in the impact angle range from 169^0 to 179^0 and within the impact angle range where the sensor can operate at an impact velocity below 15 $m.s^{-1}$, many impact angles require an impact velocity of up to 14.3 $m.s^{-1}$. When the Hall sensor is placed at P_{24}, the impact sensor has a high sensitivity as it can operate at any impact angle with an impact velocity of only 0.85 $m.s^{-1}$. When the Hall sensor is placed 12 mm from the symmetry axis of the all-ways action mechanism, the sensitivity of the impact sensor is very poor because many impact angle regions cannot operate at impact velocities below 15 $m.s^{-1}$.

The P_2 position also provides the sensor with high sensitivity and can operate in the entire contact angle area, but it is unstable and has large fluctuations. To ensure the working ability of the sensor, the Hall sensor must be placed at a position no more than 10 mm from the symmetry axis of the all-ways action mechanism, but there are still some points with low sensitivity within this range.

Figure 30 shows the sensitivity graphs of the impact sensor when placing the Hall sensor at position P_3's sampling points.

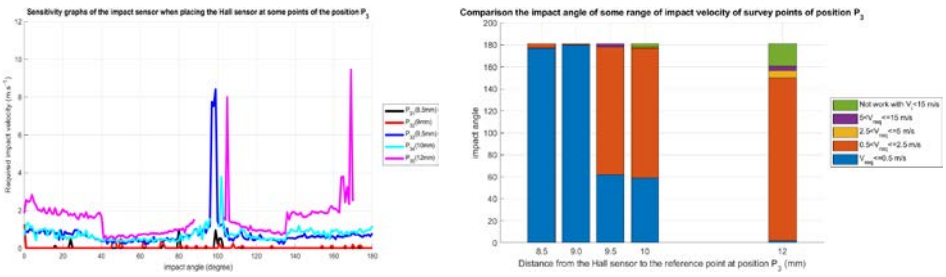

Figure 30 - The sensitivity graphs and comparison of the range of impact angles with different impact velocities when placing the Hall sensor at the position P_3

The sensitivity graphs show that when placing the Hall sensor at points P_{31} and P_{32} corresponding to distances of 8.5 mm and 9 mm from the symmetry axis of the all-ways action mechanism, the impact sensor has very high sensitivity, requiring an impact velocity of 1 $m.s^{-1}$, and it can operate at any impact angle. When placing the Hall sensor 9.5 mm away from the symmetry axis of the all-ways action mechanism, most of the impact angles still ensure good sensitivity when only needing an impact velocity of less than 2 $m.s^{-1}$ to be able to operate. However, there is a

range of impact angles from 96^0 to 100^0; the sensor has low sensitivity when needing an impact velocity of approximately 8 $m.s^{-1}$ to be able to work. Especially when the Hall is placed 10 mm from the all-ways action mechanism symmetry axis, in the impact angle range from 96^0 to 100^0, the sensor cannot work with impact velocity below 15 $m.s^{-1}$. When the distance between the Hall sensor and the all-ways action mechanism symmetry axis is 12 mm, there are two ranges of impact angle where the sensor cannot work with impact velocity below 15 $m.s^{-1}$, which are from 88^0 to 103^0 and from 170^0 to 180^0.

Figure 31 shows the sensitivity graphs of the impact sensor when placing the Hall sensor at position P_4's sampling points.

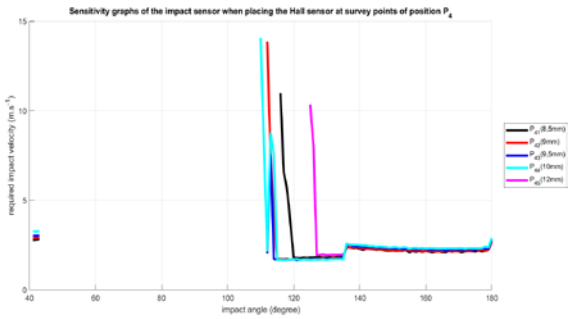

Figure 31 - Sensitivity graphs of the impact sensor when placing the Hall sensor at sampling points of position P_4

The sensitivity diagrams show that the P_4 sensor has poor sensitivity when there is a large range of impact angles at which it cannot operate, regardless of the position of the Hall sensor at the sampling points. The impact sensor can only operate in a very small area of impact angle from 41^0 to 43^0, and the area of impact angle from 110^0 to 180^0.

Study results show that positions P_2 and P_4 are unsuitable for placing the Hall sensor due to unstable sensitivity. The optimal position is P_3, located between the two inertial bodies and equidistant from the magnets, providing reliable performance within 10 mm of the mechanism's symmetry axis. Although P_1 offers lower sensitivity than P_3, it provides stable performance and can also be used. For the ring-shaped magnets in this design, the Hall sensor should be positioned 9–10 mm from the symmetry axis at P_1 or P_3 to meet sensitivity standards for the grenade fuse.

Conclusion

The paper presents a dynamic model of an all-ways action mechanism, incorporating magnetic interactions from ring magnets used

in an electro-mechanical impact sensor for grenade fuses. A combined simulation using this model and FEMM 4.2 software accurately calculates the sensor's output signal based on structural, magnetic, and velocity input parameters. The program is used to analyze how the activation threshold, inertial mass, and Hall sensor position affect sensor sensitivity. Results indicate that the activation threshold is critical, with an optimal range of 70–80 mV. The magnet's mass has minimal effect unless its density exceeds 7.55 g.cm^{-3}. The Hall sensor's location significantly impacts sensitivity, with positions P1 and P3 offering high and stable performance. It should be placed at one of these positions, within 9.5 mm of the mechanism's symmetry axis.

References

Xuan Son Bui, Duc Hung Pham, Van Gion Do, Van Bien Vo. Analysing the Sensitivity of the All-Ways Action Mechanism upon Impact on Target. 2021 International Conference on Military Technologies (ICMT), 2021 Brno. 1-5. Available at: https://doi.org/10.1109/ICMT52455.2021.9502816

Headquaters of United States Army Materiel Command 1969. *Engineering design handbook,* Washington DC, Headquaters of United statess army materiel command. Available at: https://apps.dtic.mil/sti/tr/pdf/AD0889245.pdf

Honeywell Inc. 1998. *Hall effect sensing and application*, Honeywell Inc. Available at: http://denethor.wlu.ca/pc300/projects/sensors/hallbook.pdf

BCD Semiconductor Manufacturing Limited 2010. Linear Hall-effect IC AH49E. Zi Xing Road, Shanghai ZiZhu Science-based Industrial Park, China. Available at: https://www.alldatasheet.com/datasheet-pdf/download/608101/DIODES/AH49E.html

Martin Macko, Xuan Son Bui, Kongsathit Phanthavong, Duc Hung Pham, Van Gion Do, Van Minh Do, Jiri Skala 2024. Velocity equation for grenades while impacting on dry sand media. *Defence Technology,* 35**,** 168-173. Available at: https://doi.org/10.1016/j.dt.2023.09.007

K. Phanthavong, Duc Hung Pham, Xuan Son Bui, Van Gion Do, M. Macko, Dinh Dung Tran. Analysis of Influence of Parameters on the Sensitivity of Semi-Allways Action Mechanism Using Taguchi's Method. 2023 International Conference on Military Technologies (ICMT), 23-26 May 2023 2023. 1-6. Available at: https://doi.org/10.1109/ICMT58149.2023.10171251

Arnold magnetic technologies 2021. N35-151021. *Sintered Neodymium-Iron-Boron Magnet.* Newyork: Arnold magnetic technologies. Available at: https://www.arnoldmagnetics.com/wp-content/uploads/2017/11/N35-151021.pdf

K. Yuan, G. Zhang, C. Xie, X. Song 2019. Integral definition method to solve magnetic force of axial permanent magnetic bearing. *IOP Conference Series: Materials Science and Engineering,* 504**,** 012064. Available at: https://doi.org/10.1088/1757-899X/504/1/012064

Projektovanje i analiza elektromehaničkog senzora udara sa mehanizmom dejstva u svim pravcima i Holovim senzorom

Xuan Son Bui, *Van Gion* Do, **autor za prepisku**, *Duc Hung* Pham
Le Quy Don Technical University, Faculty of Special Equipment, Hanoi, Socialist Republic of Vietnam

OBLAST: mašinstvo
KATEGORIJA (TIP) ČLANKA: originalni naučni rad

Sažetak:

Uvod/cilj: U radu se predlaže elektromehanički senzor udara za detonaciju granate koristeći mehanizam dejstva u svim pravcima u kombinaciji sa trajnim magnetima i Holovim senzorom. Nakon eksperimentalne verifikacije, koristi se matematički model za procenu uticaja strukturalnih parametara kao što su prag aktivacije, inercijalna masa i pozicija Holovog senzora na osetljivost upaljača. Studija pruža preporuke za optimalan dizajn senzora u cilju pouzdane aktivacije pod svim uglovima udara.

Metode: U studiji se koristi kombinovani pristup za rešavanje zadataka. Dinamičke jednačine mehanizma dejstva u svim pravcima rešavaju se metodom Runge-Kuta, magnetno polje se simulira softverom FEMM 4.2, a promena Holovog napona tokom vremena se analizira u cilju procene osetljivosti upaljača u uslovima udara granate.

Rezultati: Rezultati pokazuju da prag aktivacije ispod 80 mV pruža pouzdano funkcionisanje pod svim uglovima udara, sa brzinom udara koja nije već od 2,5 m/s. Masa inercijalnog tela ima značajan uticaj na osetljivost, više nego masa magneta, a pozicija Holovog senzora je ključna, jer neke pozicije pružaju stabilnu osetljivost, dok druge rezultiraju lošim performansama.

Zaključak: Hibridna metoda predstavljena u ovom radu efikasno proučava signal elektromehaničkog senzora udara koji kombinuje mehanizam dejstva u svim pravcima, trajne magnete i Holov senzor. Rezultati istraživanja predstavljaju koristan doprinos dizajnu senzora udara u upaljačima granata.

Ključne reči: elektromehanički senzor udara, mehanizam dejstva u svim pravcima, Holov sensor.

Paper received on: 25 June 2025.
Manuscript corrections submitted on: 3 October 2025.
Paper accepted for publishing on: 28 October 2025.

© 2026 The Authors. Published by Vojnotehnički glasnik / Military Technical Courier (www.vtg.mod.gov.rs).This article is an open access article distributed under the terms and conditions of the Creative Commons Attribution license (http://creativecommons.org/licenses/by/4.0/rs/